EUROPEAN ORGANIZATION FOR NUCLEAR RESEARCH

Proposal to the ISOLDE and Neutron Time-of-Flight Committee

The $d(^{30}\mathrm{Mg},p)^{31}\mathrm{Mg}$ reaction: Probing single-particle behaviour within the "island of inversion"

September 22, 2020

D. K. Sharp[1], S. J. Freeman[1], P. A. Butler[2], W. N. Catford[3], A. Ceulemans[4], L. P. Gaffney[2], C. R. Hoffman[5], R. V. F. Janssens[6,7], B. P. Kay[5], N. Kitamura[8], Th. Kröll[9], M. Labiche[10], I. Lazarus[10], G. Lotay[3], R. Lubna[11], B. Olaizola[12], T. Otsuka[8,13], O. Poleshchuk[4], R. D. Page[2], R. Raabe[4], N. Shimizu[8], T. L. Tang[5] and K. Wimmer[14]

[1]*School of Physics and Astronomy, The University of Manchester, Manchester, M13 9PL, UK*
[2]*Oliver Lodge Laboratory, University of Liverpool, Liverpool, L69 7ZE, UK*
[3]*Department of Physics, University of Surrey, Guildford, GU2 5XH, UK*
[4]*KU Leuven, Instituut voor Kern- en Stralingsfysica, 3001 Leuven, Belgium*
[5]*Physics Division, Argonne National Laboratory, Argonne, Illinois 60439, USA*
[6]*Department of Physics and Astronomy, University of North Carolina, Chapel Hill, NC 27599, USA*
[7]*Triangle Universities Nuclear Laboratory, Duke University, Durham, NC 27708, USA*
[8]*Centre for Nuclear Study, The University of Tokyo, 7-3-1 Hongo, Bunkyo-ku, Tokyo, Japan*
[9]*Institut für Kernphysik, Technische Universität Darmstadt, Germany*
[10]*STFC Daresbury Laboratory, Daresbury, Warrington, WA4 4AD, UK*
[11]*TRIUMF, 4004 Wesbrook Mall, Vancouver, British Columbia, V6T 2A3, Canada*
[12]*ISOLDE, CERN, CH-1211 Geneva 23, Switzerland*
[13]*Department of Physics and Centre for Nuclear Study, The University of Tokyo, 7-3-1 Hongo, Bunkyo-ku, Tokyo, Japan*
[14]*Instituto de Estructura de la Materia, CSIC, E-28006 Madrid, Spain*

CERN-INTC-2020-060 / INTC-P-576
22/09/2020

Spokesperson: D. K. Sharp (david.sharp@manchester.ac.uk)
Co-spokesperson: S. J. Freeman (sean.freeman@manchester.ac.uk).
ISOLDE contact: Bruno Olaizola (bruno.olaizola@cern.ch)

Abstract: We propose a measurement of the $^{30}\mathrm{Mg}(d,p)^{31}\mathrm{Mg}$ reaction in inverse kinematics, using the ISOLDE Solenoidal Spectrometer. The aim of the measurement is to characterise the neutron single-particle states in $^{31}\mathrm{Mg}$, inside the island of inversion. The neutron-adding reaction will probe spectroscopic overlaps for the $0d_{3/2}$, $0f_{7/2}$, $1p_{3/2}$ and

$1p_{1/2}$ orbitals. These data, combined with our previous data on ^{29}Mg, will describe the evolution of these orbitals, and document the shell closures they define, into the $N = 20$ island of inversion. These data will also be compared to modern shell-model predictions to ascertain how well new effective interactions are describing this evolution, in what is, theoretically, a challenging region of the nuclear chart. We request 19 shifts of beam time for this measurement.

Requested shifts: 6 days + 1 shift (19 shifts), split into 1 run over 1 year.
Installation: ISOLDE Solenoidal Spectrometer

1 Physics case

The region of nuclei around ^{32}Mg ($Z \sim 12$, $N \sim 20$) is known as the "island of inversion" (IOI) which is so-called because ground states and low-lying excitations originating from intruder configurations have been observed in these nuclei. Intruder configurations are those resulting from the promotion of one or more neutrons across a shell closure, in this case $N = 20$, generating neutron holes in the orbits below the closed shell. This phenomenon was first identified through anomalous ground-state binding energies of Mg, Na and Ne isotopes [1, 2]. The prevalence of intruder orbitals in this region is indicative of a weakening $N = 20$ shell closure as well as of increased correlations with unpaired protons.

The island of inversion has been characterised through a number of observables using different techniques, including knock-out reactions e.g., Refs. [3, 4], Coulomb excitation e.g., Refs. [5, 6, 7], β NMR e.g., Ref. [8], β decay e.g., Ref. [9], conversion electron spectroscopy [10], γ-ray spectroscopy of excited states e.g., Ref. [11] and neutron pair-transfer [12]. In the Ne, Na and Al isotopes, there is a "soft" transition to a deformed ground state through transitional nuclei where states are characterized by mixed wave functions. However, the transition has generally thought to be sharper in the Mg isotopes, with ^{30}Mg outside the island, with a ground state well described without cross-shell excitations [13, 14]. The low-energy structure of ^{31}Mg suggests there are stronger admixtures of intruder configurations [15]. However, a recent study of intermediate-energy knock-out reactions, probing the residual ^{29}Mg and ^{30}Mg nuclei [16], concludes that the cross-shell effects in this region are more complex than previously thought, in particular in ^{30}Mg. Additionally, new shell-model interactions, based on Chiral effective-field theory, describe a more transitional behaviour in terms of particle-hole excitations towards the island of inversion than previously thought [17].

In the knock-out measurements mentioned above, evidence of negative-parity states were observed in ^{30}Mg at comparatively low excitation-energy compared to ^{28}Mg. The observation of these states at low excitation are a signature of the IOI, and significant population in knock-out points to increased occupation of the corresponding orbitals. The difference between the $0d_{3/2}$ and the fp-shell single-particle energies is a measure of the size of the $N = 20$ shell closure. The size of this gap, and how it changes, characterises this unique region of the nuclear chart. However, information on the nature of the negative-parity states both approaching, and certainly inside the IOI, is lacking thus far.

The behaviour of the negative-parity states has also proven difficult to describe with established shell-model calculations, especially in the island of inversion. Often ad-hoc corrections are required in order to reproduce the observed levels. For example, in ^{30}Al the energies calculated via the WBP interaction had to be shifted by $\sim$1 MeV to properly describe the energies of the observed states [18]. Similarly in a measurement of the ^{26}Ne(d,p) reaction [19], neither the SDPF-M or WBP interactions could reproduce the energies of the negative-parity states. The recently developed EEdf1 interaction [17] has been applied to the sodium, magnesium and silicon isotopic chains and has resulted in an improved description of the properties of nuclei in this region, including ^{31}Mg, without the need for ad-hoc alterations. However, the available experimental data on this nucleus is limited, especially in terms of single-particle properties, such as single-particle energies and occupancies, and in particular for the negative-parity states that are so vital in describing the IOI.

Measurements of the nuclei approaching the island of inversion, e.g., ^{25}Ne [20] , ^{27}Ne [19], ^{26}Na [21], ^{35}Si [22] and ^{29}Mg [23], have provided important systematic information on the behaviour of the relevant orbitals. Coulomb-excitation measurements have identified the energies, spins and parities of low-lying states, including in ^{31}Mg [5]. Knock-out reactions have been successful in probing hole-structures and in deciphering initial ground-state overlaps with populated final states [15]; knowledge of the ground-state wave functions is, therefore, reasonably good. However, knock-out measurements are limited to studying hole states as cross sections to states corresponding to unoccupied orbitals are small. The states of interest here are intruder states from the shell above and, so, neutron-adding measurements are required to fully describe the behaviour of nuclei in this region. Using neutron-adding transfer reactions, we can ascertain the spin of ambiguous states and the degree of fragmentation of the single-particle orbitals towards ^{32}Mg. These data will complement the existing knock-out data on these nuclei - leading to a robust description of their single-particle behaviour.

In this proposal, we will aim to extract the distribution of the $0f_{7/2}$, $1p_{3/2}$ and $1p_{1/2}$ single-particle strengths. The expected levels, as predicted by shell-model calculations, are presented in Figure 1 for ^{31}Mg. These have been calculated using several interactions; the SDPF-MU interaction [24] is calculated for negative-parity states assuming only $1p-1h$ excitations, the FSU interaction [25], which has been developed by fitting to more two-body matrix elements and single-particle energies for the fp-shell, again only with $0p-0h$ and $1p-1h$ excitations and the aforementioned EEdf1 interaction, which includes up to $6p-6h$ and $5p-5h$ excitations for the positive- and negative-parity states, respectively. For both the SDPF-MU and FSU interactions, the single-particle energies have been shifted to reproduce the first $3/2^-$ level in ^{31}Mg. The single-particle strengths for the states of interest are predicted to be split between at least two states, one of which is likely unbound with a consequently very small γ-decay width.

The beam intensities at HIE-ISOLDE are sufficient to populate states in ^{31}Mg, via the ^{30}Mg(d,p)^{31}Mg reaction in inverse kinematics, allowing us to probe these single-neutron excitations inside the island of inversion. This reaction has been measured previously at ISOLDE using Miniball [26], at an incident beam energy of 2.2 MeV/u, and later with the T-REX set-up [27], at an incident beam energy of 2.85 MeV/u, relatively low energies for direct-reaction studies. These measurements suffered from either poor angular coverage,

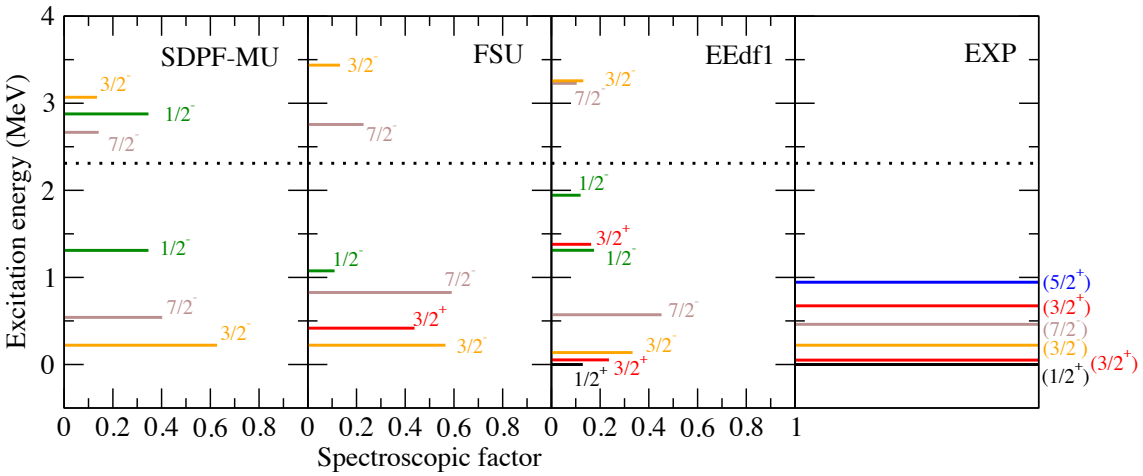

Figure 1: Shell-model calculations for single-neutron states populated in the (d,p) reaction with $S > 0.1$ using the SDPF-MU [24], FSU [28] and EEdf1 [29] interactions compared to known low-lying states. The experimental energies from the Coulomb-excitation measurements of Ref. [5] are presented for comparison - as robust spectroscopic factors are not available. The dotted line represents the neutron-separation energy. Details of the calculations can be found in the main text.

with which to make angular momentum assignments, or limited statistics, such that only the lowest-lying states were studied. Our aim is to carry out a more robust measurement of the proton yields from neutron transfer to the final states in ^{31}Mg. The resolution of the proton energy spectra is improved by using a solenoid technique, as employed with the ISOLDE Solenoidal Spectrometer (ISS), compared to traditional silicon-only setups. Coincident γ-ray measurements are therefore not required and the extraction of proton yields is not limited by the lifetime of the state. The higher beam energies now available at HIE-ISOLDE also enable a measurement at an energy more suitable for transfer reactions, both in terms of larger cross sections for certain ℓ-transfers and of more characteristic angular distributions. Most importantly, at these higher energies, the spectroscopic factors are more robust since a direct mechanism is a better assumption. Additionally, with ISS, states above the neutron separation threshold can be observed, as γ-rays are not required to extract the proton yields. This will allow us to probe not just the location of the first-excited $f_{7/2}$ and $p_{3/2,1/2}$ states, but also significant fragments of the single-particle strength that are expected to lie above the neutron threshold.

As ^{31}Mg lies just inside the island of inversion, when combined with data we obtained previously for ^{29}Mg [23], these measurements provide a picture of the evolution of the neutron orbitals moving into the IOI, mapping out the size of the energy difference between the $0d_{3/2}$ and $0f_{7/2}$ and $1p_{1/2,3/2}$ orbitals as well as the changes in neutron occupancy. These data will provide a valuable comparison in order to identify the robustness of both established and new sets of calculations and inform on the drivers of evolution in this region.

2 Experimental details

Reaction and beam energy—We propose to measure single-neutron transfer in inverse kinematics to probe the single-particle structure in neutron rich ^{31}Mg at an incident beam energy of 8 MeV/u. At this energy the angular distributions for transfer to final states of differing ℓ are more pronounced and forward peaked, compared to lower energy measurements, such that assignments of transferred angular momenta are distinct, see Fig. 3. Though the angular coverage of the array is more limited compared to measurements made at even higher energies, this beam energy is a compromise in terms of reducing levels of stable contaminants in the beam at the ISS target position. The charge states required to accelerate the ^{30}Mg beam to higher energies suffer from stable contaminants from the EBIS [30]. Therefore, the chosen beam energy is a good compromise between angular coverage, yield and levels of contamination.

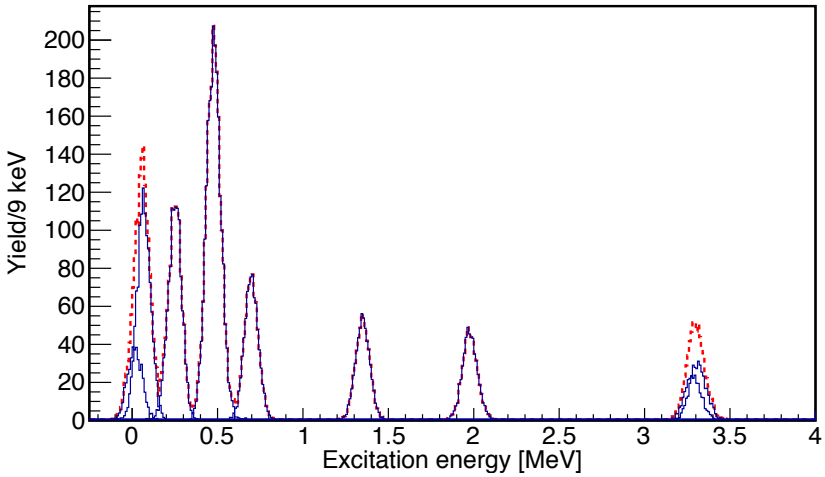

Figure 2: Simulated excitation-energy spectrum with an assumed FWHM of 100 keV. Relative yields are weighted by calculated cross sections and spectroscopic factors. Blue lines are individual peaks and the red line is the sum. Where energies of states are not known they, and all spectroscopic factors, are taken from the EEdf1 calculations.

ISOLDE Solenoidal Spectrometer—In inverse kinematics, a heavy beam is incident on a light target, in this case deuterated polyethylene (CD_2). The protons from the (d,p) reaction, at the forward centre-of-mass angles of interest, are emitted at backwards laboratory angles, relative to the incident beam direction. We intend to use ISS in order to momentum analyse the outgoing protons, measuring their energies and yields to final states in ^{31}Mg. Measurements have previously been made using the ISS for the ^{28}Mg(d,p) reaction [23], where a Q-value resolution of 145 keV FWHM was achieved, using the position-sensitive array from the HELIOS spectrometer [31], and targets in the range 90-120 μg/cm^2 thick. For the current measurement, the new silicon array and associated electronics developed by The University of Liverpool will be used. A Q-value resolution of $\sim$100 keV should be achievable with this new instrumentation. The extracted cross sections and angular distributions will be compared to calculations using the finite-range DWBA codes Ptolemy [32] and DWUCK [33], to obtain information on the ℓ value of the

final states and spectroscopic factors.

Given an expected excitation-energy resolution of 100 keV, and the level density and spacing given by the shell-model calculations in Fig. 1, one should expect to extract proton yields for most of the final states of interest without much difficulty. A simulation, including states with $S > 0.1$ as predicted using the EEdf1 interaction, is presented in Figure 2. The ground and first excited state in ^{31}Mg, separated by ∼50 keV, will not be resolved in the excitation-energy spectra but with knowledge of the shapes and widths from isolated peaks in the spectrum, and energies from previous work, it will still be possible to extract yields or fit distributions as a combination of known ℓ values. Calculations with this particular interaction also predict a doublet at 3.3 MeV, though other interactions do not. Should this truly be the case then again a combination of calculated angular distributions can be fit to the measured cross sections.

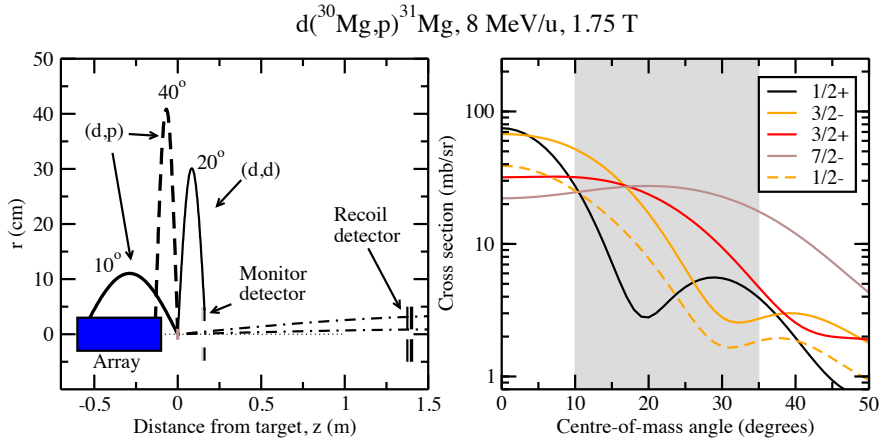

Figure 3: (Left) Proposed experimental set-up within ISS. Distances are relative to the target position. The black lines represent the trajectories of light-ions. The hatched lines represent the path of the residual beam-like nuclei. All angles are given in centre-of-mass. (Right) Angular distributions in the centre-of-mass calculated for the $1s_{1/2}$ (black), $1p_{3/2}$ (orange), $0d_{3/2}$ (red) and $0f_{7/2}$ (brown), assuming $S = 1$, at an incident beam energy of 8 MeV/u. The shaded region shows the minimum angular coverage of the array.

Experimental set-up—The configuration for the ^{30}Mg(d,p) measurement can be found in Figure 3. The silicon array will be positioned −10 cm from the target as measured to the nearest detector edge, covering a range in z from the target of −10.0 to −60.1 cm. The solenoid field will be set at 1.75 T. With these settings, protons emitted at $10° < \theta_{cm} < 35°$ will be incident on the array for all states up to 3 MeV (S_n=2.310 MeV). Elastically-scattered deuterons will be detected in an annular silicon detector positioned at $z = +16$ cm, corresponding to $\theta_{cm} = 20°$. At a position $z = +140$ cm from the target, an annular ΔE-E telescope will be located. This telescope will detect the recoiling beam-like particles in order to clean the spectra of reactions on beam contaminants and from fusion-evaporation reactions on the carbon in the target. It will also provide a timing reference for the identification of protons in the array, using their cyclotron period as a means of particle identification. A zero-degree ΔE-E silicon telescope and Faraday cup will be positioned on a moveable arm 30 cm behind the target, for measuring the

unreacted beam and determining its purity as well as for tuning purposes.

Beam time request—A beam intensity of 6×10^4 pps of ^{30}Mg has been assumed, based on the value given in the yield database, an assumption of an average proton current of $1.5\mu A$ and a total transmission efficiency to ISS of 6.2% [30]. This compares well to the 5×10^4 pps observed in IS410 and 1×10^5 pps observed in Ref. [34]. In experiment IS410 a level of ^{30}Al contamination of $\sim$ 10% was measured, which will be suppressed by the recoil detector. At this rate, there will be $\sim$150, 320 and 35 counts per day in the whole array for the states of interest, namely the strongest $p_{3/2}$ (S=0.4), $f_{7/2}$ (S=0.4) and $p_{1/2}$ (S=0.2) states, respectively, using the spectroscopic factors given in the shell-model calculations. The array has an efficiency of 70% in the azimuthal angle and 94% in the theta angle. The CD_2 targets will be $\sim$100 μg/cm^2 thick. Cross sections were estimated using the finite-range DWBA code Ptolemy and optical-model parameters of An and Cai [35] and Koning and Delaroche [36] for the deuteron and proton, respectively.

The aim here is to study the fragmentation of single-particle strength and so weak fragments are of interest. **18 shifts** of ^{30}Mg beam on target would be required to achieve yields of at least 200 counts in $p_{3/2}$ or $f_{7/2}$ states with $S = 0.1$. These counts would be distributed amongst eight angular bins (25 counts per bin on average), allowing extraction of spectroscopic factors with a minimum uncertainty of 20%. A $p_{1/2}$ state with $S = 0.1$ would have 100 counts after the requested number of shifts, and so the uncertainty of the spectroscopic factors would be larger for these states. This can be mitigated to some extent by using a more coarse angular binning for weak states. We also request a further **1 shift** in order to optimise the radioactive beam into the spectrometer.
Summary of requested protons: 19 shifts of protons are requested for this measurement.

References

[1] C. Thibault, *et al.,* Phys. Rev. C **12**, 644 (1975).
[2] E. K. Warburton, J. A. Becker, and B. A. Brown Phys. Rev. C **41**, 1147 (1990).
[3] A. Gade, *et al.,* Phys. Rev. Lett. **99**, 072502 (2007).
[4] P. Fallon, *et al.,* Phys. Rev. C **81**, 041302 (2010).
[5] M. Seidlitz, *et al.,* Phys. Rev. C **89**, 024309 (2014).
[6] M. Seidlitz, *et al.,* Phys. Lett. B **700**, 181 (2011).
[7] J. A. Church, *et al.,* Phys. Rev. C **72**, 054320 (2005).
[8] M. Kowalska, *et al.,* Eur. Phys. J A **25**, s01, 193 (2005).
[9] F. Maréchal, *et al.,* Phys. Rev. C **76**, 059902 (2007).
[10] E. Schwerdtfeger, *et al.,* Phys. Rev. Lett. **103**, 012501 (2009).
[11] A. N. Deacon, *et al.,* Phys. Rev. C **82**, 034305 (2010).
[12] K. Wimmer, *et al.,* Phys. Rev. Lett. **105**, 252501 (2010).
[13] B. V. Pritychenko, *et al.,* Phys. Lett. B **461**, 322 (1999).
[14] O. Niedermaier *et al.,* Phys. Rev. Lett. **94**, 172501 (2005).
[15] J. R. Terry, *et al.,* Phys. Rev. C **77**, 014316 (2008).
[16] B. Fernández-Domínquez, *et al.,* Phys. Lett. B **779**, 124 (2018).

[17] N. Tsunoda, *et al.,* Phys. Rev. C. **95**, 021304(R) (2017).
[18] D. Steppenbeck, *et al.,* Nucl. Phys. A. **847**, 149 (2010).
[19] S. M. Brown, *et al.,* Phys. Rev. C **85**, 011302 (2012).
[20] W. N. Catford, *et al.,* Phys. Rev. Lett. **104**, 192501 (2010).
[21] G. L. Wilson, *et al.,* Phys. Lett. B **381**, 417-423 (2014).
[22] G. Burgunder, *et al.,* Phys. Rev. Lett. **759**, 042502 (2014).
[23] D. K. Sharp, *et al.,* IS621
[24] Y. Utsuno (Private communication).
[25] R. Lubna, *et al.,* Phys. Rev. C. **100**, 034308 (2019).
[26] M. Pantea. PhD Thesis, Technische Universität Darmstadt, (2005).
[27] V. Bildstein. PhD Thesis, Technische Universität München, (2010).
[28] R. Lubna, (Private communication).
[29] N. Shimizu, (Private communication).
[30] J. A. R. Rodriguez (Private communication).
[31] A. H. Wuosmaa, *et al.,* Nucl. Instrum. Meth. A, **580**, 1290 (2007).
[32] M. H. Macfarlane and S. C. Pieper, ANL-76-11 Rev. 1, ANL Report (1978).
[33] P. D. Kunz, University of Colorado Report COO-535-606.
[34] N. Imai, *et al.,* Phys. Rev. C **90**, 011302(R) (2014).
[35] H. An and C. Cai Phys. Rev. C **73**, 054605 (2006).
[36] A. J. Koning and J. P. Delaroche Nuc. Phys. A. **713**, 231 (2003).

Appendix 1: Status of the experiment IS621

This information is to provide the INTC members with the status of the $d(^{28}\mathrm{Mg},p)^{29}\mathrm{Mg}$ measurement (IS621) made with ISS before LS2, which is connected to the current proposal, to provide insight in to the performance of ISS. This was one of two measurements made with ISS in an early-exploitation arrangement, using the position-sensitive array from the HELIOS spectrometer at Argonne National Laboratory. The other being a measurement of the $d(^{206}\mathrm{Hg},p)^{207}\mathrm{Hg}$ reaction that has been published in Physical Review Letters.

The analysis of the data is now completed and a manuscript is in preparation. The analysis has taken longer than initially anticipated due to checks performed to assess the robustness of the DWBA reaction modelling used to extract spectroscopic factors for the unbound states that were populated in the reaction. The excitation-energy spectrum for the residual states in ^{29}Mg is given in Figure 4. This shows the sum of all detectors on the array, with a FWHM for the bound states of ∼145 keV. States were populated up to ∼6 MeV in ^{29}Mg. Measured angular distributions for states up to 4.36 MeV are shown in Figure 5, compared to those calculated using the finite-range DWBA code DWUCK. The highest energy states were only measured at a single angle so no distributions could be extracted.

Spectroscopic factors have been extracted for all states and a comparison to modern sets of shell-model calculations have been made, Figure 6. These data are used to describe the evolution of the $d_{3/2}$, $f_{7/2}$ and $p_{3/2,1/2}$ orbitals along the $N = 17$ isotones - towards ^{25}O. A comparison of the measured single-particle centroids to those calculated using the FSU interaction are given in Figure 7. Deviations of the calculations from the experimental data point to the influence of effects not included in shell-model calculations, such as weak-binding effects on p-orbitals.

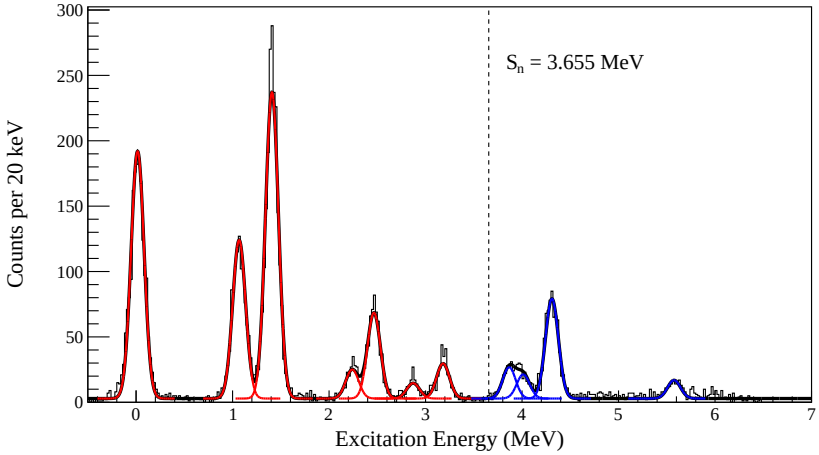

Figure 4: Excitation spectrum, with fitted gaussians, for measurement of $d(^{28}\mathrm{Mg},p)^{29}\mathrm{Mg}$ reaction with ISS. This represents a sum of all detectors on the array with a measured FWHM of ∼145 keV.

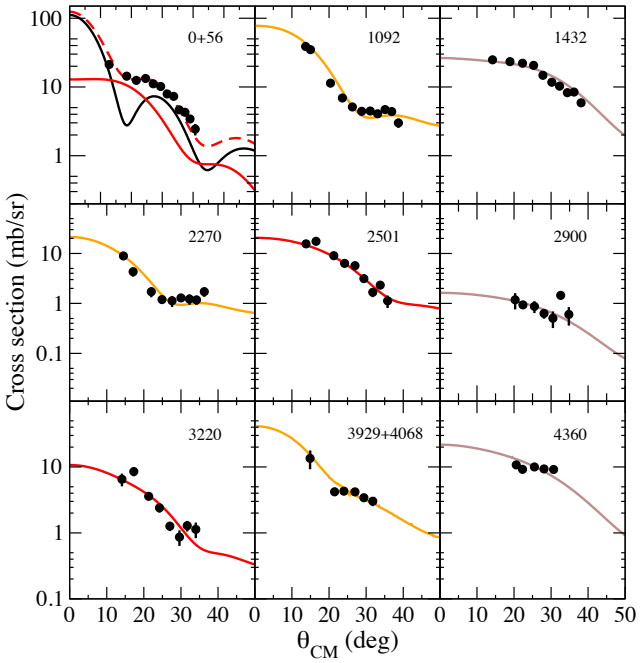

Figure 5: Angular distributions for states observed in the ^{28}Mg(d,p)^{29}Mg reaction. The solid lines are DWBA calculations for the assigned state with $\ell = 0$ (black), 1 (orange), 2 (red) and 3 (brown). The dotted line for the ground-state doublet denotes a combination of the two distributions have been fitted.

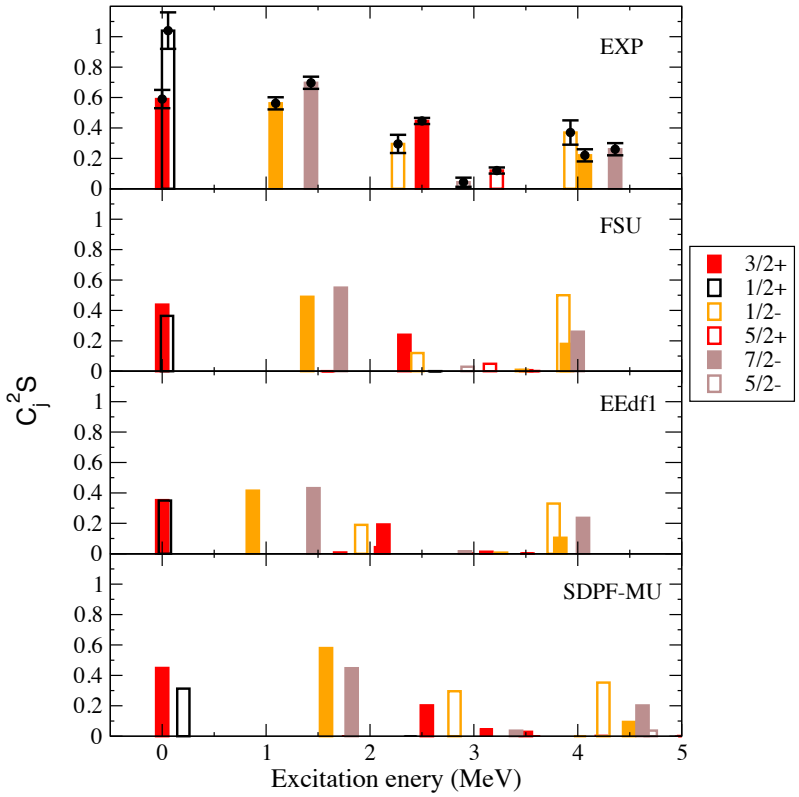

Figure 6: SFs extracted from the present work (EXP) for states with $J^\pi = 1/2^+$ (unfilled black), $1/2, 3/2^-$ (unfilled/filled orange), $3/2, 5/2^+$ (filled/unfilled red) and $5/2, 7/2^-$ (unfilled/filled brown). The experimental errors shown are statistical. SFs from shell-model calculations are given for a number of interactions.

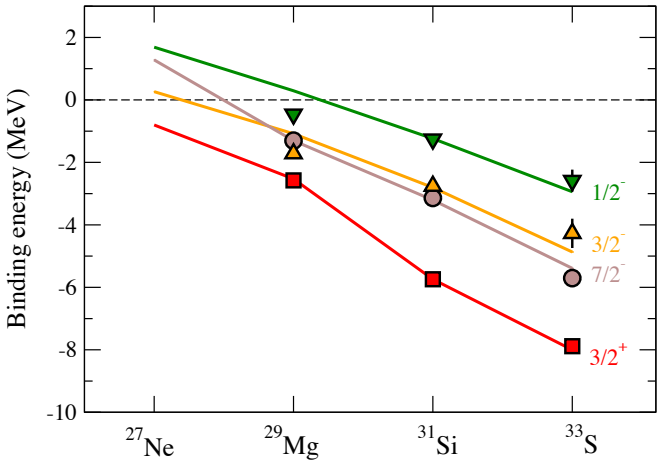

Figure 7: Single-particle energy centroids for states with $J^\pi = 3/2^+$ ($\square$), $7/2^-$ ($\bigcirc$), $3/2^-$ ($\triangle$) and $1/2^-$ ($\triangledown$) in the $N = 17$ isotones. Lines represent ESPE's calculated from the FSU interaction, shifted on to the respective centroid at ^{31}Si.

Appendix 2

DESCRIPTION OF THE PROPOSED EXPERIMENT

The experimental setup comprises: The ISOLDE Solenoidal Spectrometer

Part of the	Availability	Design and manufacturing
ISOLDE Solenoidal Spectrometer	☒ Existing	☒ To be used without any modification ☐ To be modified
	☐ New	☐ Standard equipment supplied by a manufacturer ☐ CERN/collaboration responsible for the design and/or manufacturing

HAZARDS GENERATED BY THE EXPERIMENT (if using fixed installation:) Hazards named in the document relevant for the fixed ISS installation.

Additional hazards:

Hazards			
Thermodynamic and fluidic			
Pressure			
Vacuum			
Temperature			
Heat transfer			
Thermal properties of materials			
Cryogenic fluid			
Electrical and electromagnetic			
Electricity			
Static electricity			
Magnetic field	1.75 T		
Batteries			
Capacitors			
Ionizing radiation			
Target material	Deuterated polyethylene (50-400 μg/cm^2)		
Beam particle type	^{30}Mg		
Beam intensity	6×10^4		
Beam energy	8 MeV/u		
Cooling liquids			
Gases			
Calibration sources:	☒		
• Open source	☒ (α calibrations source 4236RP)		
• Sealed source			

• Isotope	^{148}Gd, ^{239}Pu, ^{241}Am, ^{244}Cm		
• Activity	1 kBq, 1 kBq, 1 kBq, 1 kBq = 4 kBq		
Use of activated material:			
• Description			
• Dose rate on contact and in 10 cm distance			
• Isotope			
• Activity			
Non-ionizing radiation			
Laser			
UV light			
Microwaves (300MHz-30 GHz)			
Radiofrequency (1-300 MHz)			
Chemical			
Toxic			
Harmful			
CMR (carcinogens, mutagens and substances toxic to reproduction)			
Corrosive			
Irritant			
Flammable			
Oxidizing			
Explosiveness			
Asphyxiant			
Dangerous for the environment			
Mechanical			
Physical impact or mechanical energy (moving parts)			
Mechanical properties (Sharp, rough, slippery)			
Vibration			
Vehicles and Means of Transport			
Noise			
Frequency			
Intensity			

Physical			
Confined spaces			
High workplaces			
Access to high workplaces			
Obstructions in passageways			
Manual handling			
Poor ergonomics			

Hazard identification:

Average electrical power requirements (excluding fixed ISOLDE-installation mentioned above): N/A